MATHEMATICAL BIOSCIENCES
AND ENGINEERING
Volume **6**, Number **1**, January **2009**

doi:10.3934/mbe.2009.6.145

pp. **145–172**

THE DYNAMICS OF A SIMPLE LAISSEZ-FAIRE MODEL WITH TWO PREDATORS

Gunog Seo and Mark Kot

University of Washington, Applied Mathematics, Box 352420
Seattle, WA 98195-2420, USA

(Communicated by Yang Kuang)

Abstract. In this paper, we study the dynamics of a laissez-faire predator–prey model with both a specialist and a generalist predator. We analyze the stabilities of equilibria by performing linearized stability analyses. We then reexamine the stability of the equilibrium where the prey and predator coexist by constructing a Lyapunov function. If we hold the generalist predator population constant, treating it as a bifurcation parameter, we show that our model can possess multiple (up to three) limit cycles that surround an equilibrium in the interior of the first quadrant. Our model shows rich dynamics including fold, transcritical, pitchfork, Hopf, cyclic-fold, and Bautin bifurcations as well as heteroclinic connections. If we instead vary the generalist predator population slowly across bifurcations, the model exhibits bursting behavior as it alternates between a repetitive spiking phase and a quiescent phase.

1. **Introduction.** Predators may be divided into two large groups, *specialists* and *generalists* [13, 43]. Specialist predators rely on a single food source, while generalist predators feed on a variety of abundant prey. Andersson and Erlinge [2] classified predators into three groups based on the degree of specialization and mobility: resident specialists, nomadic specialists, and generalists. However, in this paper, we will only refer to two groups of predators, specialists and generalists.

Many experimental and theoretical studies have analyzed regular multi-annual cycles of rodent population in northern Fennoscandia (see, for example, [13, 14, 23, 24, 32, 43]). Hanski et al. [13] have suggested that specialist predators contribute to population cycles while generalist predators have a stabilizing effect. The number of generalist predators increases from north to south and in southern regions small rodents exhibit seasonal changes in population size without more pronounced multi-annual cycles.

If we disregard age, size, and time lags, the interactions among a specialist predator, a generalist predator, and their prey in a homogeneous environment may be modeled mathematically by

$$\frac{dN}{dT} = rN\left(1-\frac{N}{K}\right) - \Phi_{\mathrm{II}}(N)P - \Phi_{\mathrm{III}}(N)G, \tag{1a}$$

$$\frac{dP}{dT} = P\,\Psi(N,P), \tag{1b}$$

2000 *Mathematics Subject Classification.* 34D05, 34D20, 92D25.

Key words and phrases. laissez-faire predator–predator–prey model, Bautin bifurcation, heteroclinic connection, bursting.

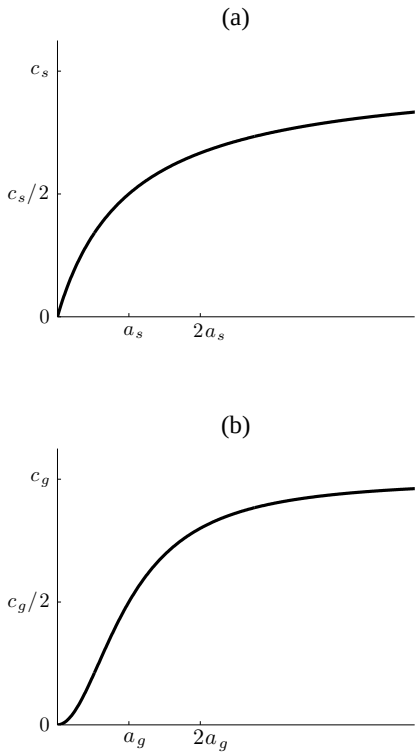

FIGURE 1. Holling (a) type II and (b) type III functional responses. The abscissa and ordinate represent the prey density and the number of prey eaten per predator per unit time. The parameter a_s and a_g are half-saturation constants and c_s and c_g are maximum per-capita consumption rates. The subscripts s and g signify the specialist and generalist predators.

with

$$\Phi_{\mathrm{II}}(N) = \frac{c_s N}{N + a_s}, \qquad \Phi_{\mathrm{III}}(N) = \frac{c_g N^2}{N^2 + a_g^2}. \tag{2}$$

N and P are the prey and the specialist predator populations at time T. G represents the generalist predator population. We will start by treating G as a parameter. $\Phi_{\mathrm{II}}(N)$ and $\Phi_{\mathrm{III}}(N)$ are functional responses. $\Psi(N, P)$ is the specialist predator's numerical response. We will say more about $\Phi_{\mathrm{II}}(N)$, $\Phi_{\mathrm{III}}(N)$, and $\Psi(N, P)$ shortly.

In prey growth-equation (1a), the prey population grows logistically, in the absence of predators, with intrinsic rate of growth r and carrying capacity K. In the presence of predators, however, the growth of the prey is hindered by both the specialist and generalist predators at rates proportional to their functional responses, $\Phi_{\mathrm{II}}(N)$ and $\Phi_{\mathrm{III}}(N)$. The subscripts, II and III, signify the type II and the type III functional responses identified by Holling [17, 18].

A functional response specifies the rate at which prey are consumed, per predator, as a function of the prey density [41]. In a type II functional response (Fig. 1(a)),

the predation rate increases as the prey density grows, but eventually levels off due to the predator's handling time. In a type III functional response (Fig. 1(b)), characterized by an S-shaped curve, the predation rate is convex at low prey density, but concave at high prey density. We assume that the specialist and generalist predators possess Holling type II and type III functional responses: many generalist predators that have a stabilizing effect are characterized by a type III functional response. In each functional response, the subscripts s and g signify the specialist and generalist predators. The parameter a (a_s or a_g) is referred to as the half-saturation constant and is the number of prey at which the per-capita predation rate is half of its maximum, c_s or c_g.

In equation (1b), $\Psi(N,P)$, the per-capita growth rate of the specialist predator population, is the numerical response (e.g., [47]). There are two forms of the numerical response for the specialist predator that are frequently used [14, 32, 47]:

$$\Psi(N,P) \;=\; s\left(1-\frac{P}{qN}\right) \tag{3}$$

and

$$\Psi(N,P)=\Psi(N) \;=\; \frac{b}{c_s}\,\Phi_{\mathrm{II}}(N)-m, \tag{4}$$

where all parameters, s, q, b, and m, are positive constants.

The numerical response in equation (3) was introduced by Leslie [28]. The predator population grows logistically with intrinsic rate of growth s and a carrying capacity, qN, that is proportional to the number of prey. This predator growth-equation clearly shows that the per-capita growth rate ($1/P\ dP/dT$) is a monotonically decreasing function of P. Predator equation (3) is often applied when predators are territorial [14, 43].

Equation (4) is called a laissez-faire predator equation [5, 47] since the specialist predators do not interfere with each other. The predator population grows by converting the consumed prey into new predators with efficiency b/c_s, where b is the maximum per-capita birth rate of the specialist predators and c_s is the maximum per-capita consumption rate. In the absence of prey, however, the specialist predators decline exponentially with per-capita mortality rate m.

In this paper, we study a simple laissez-faire predator–predator–prey model with both specialist and generalist predators,

$$\frac{dN}{dT} \;=\; rN\left(1-\frac{N}{K}\right)-\Phi_{\mathrm{II}}(N)P-\Phi_{\mathrm{III}}(N)G, \tag{5a}$$

$$\frac{dP}{dT} \;=\; P\left(\frac{b}{c_s}\,\Phi_{\mathrm{II}}(N)-m\right), \tag{5b}$$

where G is assumed to be a parameter. In analogy with laissez-faire predator equation (5b), we will call model (5) a laissez-faire predator–predator–prey model.

Compared to the many studies of predator–predator–prey models with the Leslie numerical response (see, for example, [13, 30, 43, 46]), there have been few studies of predator–predator–prey models with laissez-faire numerical responses and no detailed analysis of the underlying dynamics. We believe our analysis serves as a useful contrast to similar models with Leslie numerical responses and as a baseline for future work that considers more complicated models.

We first start by nondimensionalizing system (5). Introducing dimensionless variables,

$$x = \frac{N}{a_s}, \quad y = P\,\frac{c_s}{ra_s}, \quad z = G\,\frac{c_g}{ra_g}, \quad t = rT, \tag{6}$$

reduces system (5) to

$$\frac{dx}{dt} = x\left(1-\frac{x}{\gamma}\right) - \frac{x}{1+x}\,y - \frac{\delta x^2}{\delta^2+x^2}\,z, \tag{7a}$$

$$\frac{dy}{dt} = \alpha y\left(\frac{x}{1+x} - \beta\right), \tag{7b}$$

where

$$\alpha = \frac{b}{r}, \quad \beta = \frac{m}{b}, \quad \gamma = \frac{K}{a_s}, \quad \delta = \frac{a_g}{a_s}. \tag{8}$$

Nondimensionalized system (7) can be rewritten as

$$\frac{dx}{dt} = \phi(x)\,(f(x) - y), \tag{9a}$$

$$\frac{dy}{dt} = \alpha y\,(\phi(x) - \beta), \tag{9b}$$

with

$$\phi(x) = \frac{x}{1+x} \tag{10}$$

and

$$f(x) = (1+x)\left(1 - \frac{x}{\gamma} - \frac{\delta x}{\delta^2+x^2}\,z\right). \tag{11}$$

Throughout this paper, we will usually assume that $\alpha > 0$, $0 < \beta < 1$, $\gamma > 2$, and $0 < 2\delta < \gamma$.

This paper consists of four sections. In Section 2, we study nondimensionalized system (9) treating z as a time-independent parameter. We carry out linearized stability analyses for all equilibria. We mainly focus on the stability of an equilibrium point in the interior of the first quadrant that we call the coexistence equilibrium. We then reinvestigate the stability of the coexistence equilibrium by constructing a Lyapunov function. We report on numerical studies that show that system (9) can possess up to three limit cycles that surround the coexistence equilibrium. These multiple limit cycles arise by means of a local Hopf bifurcation or a global cyclic-fold bifurcation. Moreover, we observe a heteroclinic orbit that connects two saddle points. In Section 3, we apply sinusoidal forcing to z. For slow forcing, we observe bursting phenomena where the fast variables, $x(t)$ and $y(t)$, undergo successive alternations between active spike-like oscillations and a silent phase that is nearly at steady state. Finally, in Section 4, we summarize our results and consider general interpretations of our results from an ecological viewpoint.

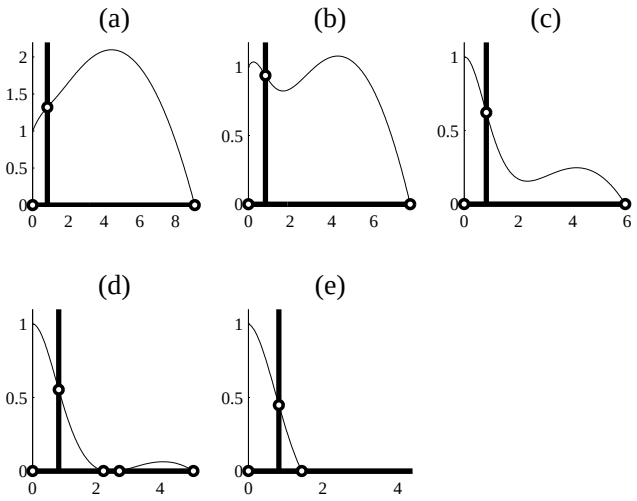

FIGURE 2. Possible null-clines for system (9) with the parameter values, $\alpha = 0.2$, $\beta = 0.45$, $\gamma = 10$, $\delta = 1.75$, and different values of z: (a) $z = 0.5$, (b) $z = 1.05$, (c) $z = 1.5$, (d) $z = 1.6$, (e) $z = 1.75$. Thin curves are the prey null-clines and thick lines are the predator null-clines. Circles indicate equilibrium points.

2. **Laissez-faire model with a time-independent parameter z.**

2.1. **Analytic studies.**

2.1.1. *Linearized stability analyses of equilibria.* Fig. 2 illustrates several possible zero-growth isoclines (or null-clines) where either the prey or specialist-predator growth rates are zero. At the intersection of the prey and specialist predator null-clines, we find equilibria, points where both dx/dt and dy/dt are zero.

Assuming $\alpha > 0$, $0 < \beta < 1$, $\gamma > 2$, and $0 < 2\delta < \gamma$, system (9) has at most five equilibria,

$$E_0 = (0,\ 0), \quad E_{1,i} = (k_i,\ 0), \quad E_2 = (x^*,\ f(x^*)), \tag{12}$$

where $f(k_i) = 0$ $(i = 1, 2, 3)$ and $x^* = \beta/(1 - \beta)$. Please note that we assign $E_{1,i}$ $(i = 1, 2, 3)$ from left to right. For example, if we have one equilibrium on the positive x-axis, we call the equilibrium $E_{1,1}$. If three equilibria appear on the positive x-axis, we designate them as $E_{1,1}$, $E_{1,2}$, and $E_{1,3}$ $(0 < k_1 < k_2 < k_3)$. Through our analyses, we will also assume $x^* < \max(k_i) = \hat{k}$ $(i = 1, 2, 3)$. We will say more about $E_{1,i}$ later in this section.

In order to analyze the stability of an equilibrium, we may use the Jacobian (or community) matrix if the eigenvalues of the Jacobian evaluated at the equilibrium have nonzero real parts. The Jacobian matrix for system (9) is

$$J = \begin{pmatrix} \phi'(x)\,(f(x) - y) + \phi(x)f'(x) & -\phi(x) \\ \alpha y \phi'(x) & \alpha\,(\phi(x) - \beta) \end{pmatrix}. \tag{13}$$

At E_0, where both prey and specialist predators are extinct, the Jacobian is

$$J = \begin{pmatrix} 1 & 0 \\ 0 & -\alpha\beta \end{pmatrix} \tag{14}$$

and the eigenvalues are the components on the diagonal,

$$\lambda_1 = 1, \quad \lambda_2 = -\alpha\beta. \tag{15}$$

Hence, E_0 is a saddle point because the two real eigenvalues are of opposite sign.

The Jacobian at $E_{1,i}$ $(i = 1, 2, 3)$, where only the prey survives, is

$$J = \begin{pmatrix} \phi(k_i)f'(k_i) & -\phi(k_i) \\ 0 & \alpha\left(\phi(k_i) - \beta\right) \end{pmatrix} \tag{16}$$

and the eigenvalues are

$$\lambda_1 = \phi(k_i)f'(k_i), \quad \lambda_2 = \alpha(\phi(k_i) - \beta). \tag{17}$$

The stability of $E_{1,i}$ can be determined by the signs of eigenvalues λ_1 and λ_2. That is, $E_{1,i}$ is a stable (unstable) node/focus if the signs of both eigenvalues are negative (positive). If the eigenvalues are of opposite sign, $E_{1,i}$ is a saddle point, which is unstable. With our assumptions, α and $\phi(k_i)$ are positive: $\phi(x)$ is an increasing function of x. Thus, $E_{1,i}$ is a stable node/focus if $f'(k_i) < 0$ and $k_i < x^*$, an unstable node/focus if $f'(k_i) > 0$ and $k_i > x^*$, and a saddle point if $f'(k_i)\,(k_i - x^*) < 0$.

The values of k_i's can be obtained by solving $f(x) = 0$. We must thus consider the cubic equation

$$x^3 - \gamma x^2 + (\delta^2 + \gamma\delta z)x - \gamma\delta^2 = 0. \tag{18}$$

Using the discriminant

$$\Delta = Q^3 + R^2 \tag{19}$$

with

$$Q = \frac{3\left(\delta^2 + \gamma\delta z\right) - \gamma^2}{9}, \quad R = \frac{\gamma\left\{9(2\delta^2 - \gamma\delta z) + 2\gamma^2\right\}}{54}, \tag{20}$$

we find that there are three cases.

If $\Delta > 0$, cubic equation (18) has a unique positive root. Because $f'(k_1) < 0$ and $k_1 > x^*$, the two eigenvalues in (17) are of opposite sign. Hence, $E_{1,1} = (k_1, 0)$ is a saddle point. If $\Delta < 0$, equation (18) has three positive roots, so that our system has three positive x-axis equilibria, $E_{1,1}$, $E_{1,2}$, and $E_{1,3}$ with $0 < k_1 < k_2 < k_3$. Please see Table 1 for more details about the stability of these equilibria. Finally, if $\Delta = 0$, at least two roots coincide. In this case, we expect a fold bifurcation, also known as a tangent, saddle-node, or blue-sky bifurcation.

At coexistence equilibrium E_2, where both prey and specialist predators coexist, the Jacobian is

$$J = \begin{pmatrix} \beta f'(x^*) & -\beta \\ \alpha f(x^*)\phi'(x^*) & 0 \end{pmatrix} \tag{21}$$

and the characteristic equation is

$$\lambda^2 - \beta f'(x^*)\lambda + \alpha\beta f(x^*)\phi'(x^*) = 0. \tag{22}$$

Since the quantities β and $\alpha\beta f(x^*)\phi'(x^*)$ are positive, the Routh–Hurwitz criterion guarantees that equilibrium E_2 is stable if $f'(x^*)$ is negative.

TABLE 1. Equilibria and their stability

Equilibrium		**Coordinates**	**Stability / Coordinates**	
	E_0	$(0,0)$	Saddle	
	E_2	$(x^*, f(x^*))$	Stable if $f'(x^*) < 0$ Unstable if $f'(x^*) > 0$	
$\Delta > 0:$	$E_{1,1}$	$(k_1, 0)$	Saddle	
$\Delta < 0:$	$E_{1,i}$ $(i = 1,2,3)$	$(k_i, 0)$	$x^* < k_1 < k_2 < k_3$	$E_{1,1}$: Saddle $E_{1,2}$: Unstable Node $E_{1,3}$: Saddle
			$k_1 < x^* < k_2 < k_3$	$E_{1,1}$: Stable Node $E_{1,2}$: Unstable Node $E_{1,3}$: Saddle
			$k_1 < k_2 < x^* < k_3$	$E_{1,1}$: Stable Node $E_{1,2}$: Saddle $E_{1,3}$: Saddle

2.1.2. *Stability analysis by a Lyapunov function.* To study the stability and basin of attraction of equilibrium $E_2 = (x^*, f(x^*))$, we perform Harrison's gedankenexperiment [15] and introduce the Lyapunov function

$$V(x,y) \;=\; \alpha \int_{x^*}^{x} \left(1 - \frac{\beta}{\phi(u)}\right) du + \int_{y^*}^{y} \left(1 - \frac{f(x^*)}{u}\right) du. \tag{23}$$

Equation (23) can also be rewritten as

$$V(x,y) \;=\; V_1(x) + V_2(y), \tag{24}$$

where

$$V_1(x) = \alpha \left[(1-\beta)(x - x^*) - \beta \ln \left|\frac{x}{x^*}\right|\right] \tag{25}$$

and

$$V_2(y) \;=\; (y - y^*) - f(x^*) \ln \left|\frac{y}{y^*}\right|. \tag{26}$$

The function $V(x,y)$ is zero at the coexistence equilibrium E_2 and is positive for all positive $x(t)$ and $y(t)$ except at E_2. If the inner product of the gradient of $V(x,y)$, $\nabla V(x,y)$, with the vector field is strictly negative,

$$\nabla V(x,y) \cdot \left(\frac{dx}{dt}, \frac{dy}{dt}\right) \;=\; \frac{\partial V}{\partial x}\,\frac{dx}{dt} + \frac{\partial V}{\partial y}\,\frac{dy}{dt} \;=\; \frac{dV}{dt} \;<\; 0, \tag{27}$$

in a neighborhood of E_2, then the vector field points inward on the level curves of $V(x,y)$. Thus, any neighborhood that satisfies (27) is a subset of the basin of attraction.

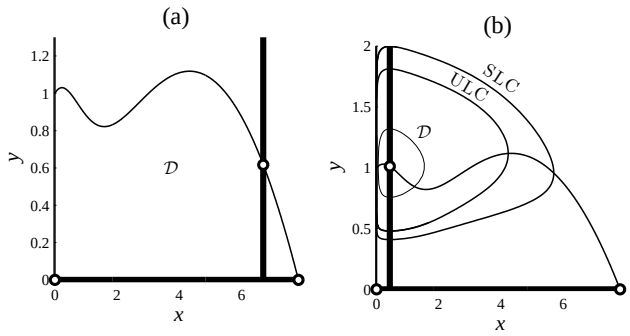

FIGURE 3. A figure illustrating (a) isoclines consistent with global asymptotic stability and (b) a subset of the domain of attraction ($\mathcal{D}$) for an equilibrium where both prey and predators coexist in laissez-faire model (9). Equilibria (circles) can be found at the intersections of the prey null-clines (thin lines) and the predator null-clines (thick lines). ULC and SLC signify unstable and stable limit cycles: (a) $\beta = 0.87$ and (b) $\beta = 0.3$ with $\alpha = 0.1$, $\gamma = 10$, $\delta = 1.7$, and $z = 1.05$.

Differentiating either (23) or (24) with respect to time, we have

$$\dot{V}\left(=\frac{dV}{dt}\right) \;=\; \alpha\,(\phi(x)-\beta)\,(f(x)-f(x^*))\,. \tag{28}$$

The time derivative $\dot{V}$ is strictly negative in a neighborhood of the coexistence equilibrium E_2 if $f(x) > f(x^*)$ for $x < x^*$ and $f(x) < f(x^*)$ for $x > x^*$. With these sufficient conditions, we can determine a subset of the domain of attraction of coexistence equilibrium E_2,

$$\mathcal{D} \;=\; \{(x,y) \mid V(x,y) < u\} \tag{29}$$

with

$$u \;=\; \min\{V(x_L, f(x^*)),\; V(x_H, f(x^*)),\; V(x^*, 0),\; V(x^*, +\infty)\} \tag{30}$$

where x_L and x_H are the smallest and largest values such that

$$f(x) \;\geq\; f(x^*)\,, \quad \text{for } x_L < x < x^*\,, \tag{31a}$$

$$f(x) \;\leq\; f(x^*)\,, \quad \text{for } x^* < x < x_H\,. \tag{31b}$$

Fig. 3(a) shows a case in which the entire interior of the first quadrant is the basin of attraction of E_2. In contrast, Fig. 3(b) shows a case in which $\mathcal{D}$ is not the entire basin of attraction, or rather, underestimates this basin. Please note that $\mathcal{D}$, in Fig. 3(b), is only a subset of the basin of attraction: all trajectories starting inside the unstable limit cycle converge to stable equilibrium E_2.

2.2. **Numerical observations.** Laissez-faire model (9) possesses at most five equilibria for $\alpha > 0$, $\gamma > 2$, $0 < 2\delta < \gamma$, and $0 < \beta < f(\hat{k})$, where $\hat{k} = \max(k_i)$, $i = 1, 2, 3$. We have found that extinction equilibrium, E_0, is a saddle point, and

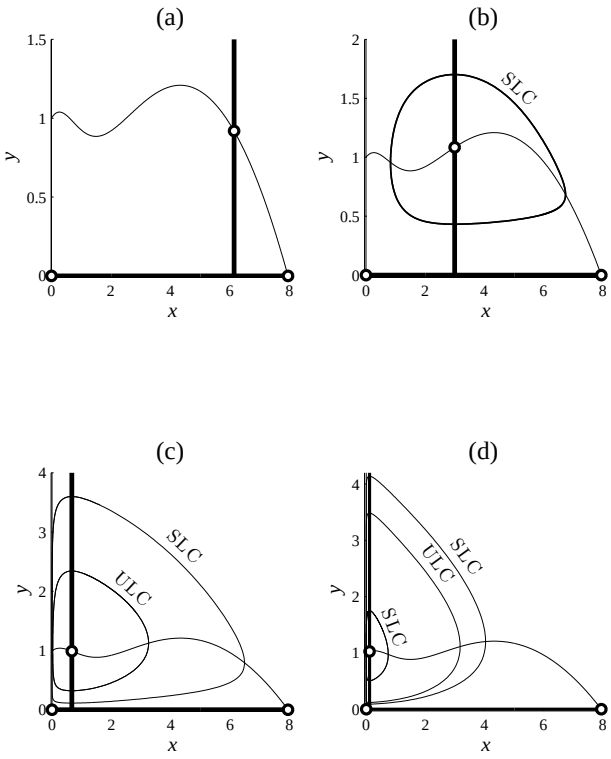

FIGURE 4. Phase portraits and null-clines for system (9) with $\alpha = 0.5$, $\gamma = 10$, $\delta = 1.7$, and $z = 1$ with (a) $\beta = 0.86$, (b) $\beta = 0.75$, (c) $\beta = 0.4$, and (d) $\beta = 0.1$. Equilibria (circles) occur at the intersections of the prey null-clines (thin lines) and the predator null-clines (thick lines). Decreases in β cause the specialist predator null-cline to move leftward. As we decrease β, the prey and the specialist predators coexist either at equilibrium or in an oscillatory manner. SLC and ULC signify a stable and an unstable limit cycle.

the stability of coexistence equilibrium E_2 is determined by the sign of $f'(x^*)$. E_2 is stable (unstable) if $f'(x^*)$ is negative (positive). For $E_{1,i}$ $(i = 1, 2, 3)$, we considered three cases according to discriminant (19) for cubic equation (18).

In the following two subsections, we highlight two striking features observed in model (9): the occurrence of multiple (up to three) limit cycles and the occurrence of a heteroclinic connection.

2.2.1. *Multiple limit cycles.* In Fig. 4(a), for any initial conditions, the system returns to stable coexistence equilibrium E_2. As we decrease the parameter β, the predator vertical null-cline crosses from the right to the left of the the right hump of

the prey null-cline (Fig. 4(b)). E_2 loses its stability and a stable limit cycle emerges around E_2 in a super-critical Hopf bifurcation. As we continue to decrease β, the predator null-cline passes through the valley of the prey null-cline, E_2 regains its stability, and an unstable limit cycle arises in a reverse sub-critical Hopf bifurcation (Fig. 4(c)). Both E_2 and the unstable limit cycle lie inside the original stable limit cycle. For small β, the predator null-cline comes close to the y-axis (Fig. 4 (d)). The coexistence equilibrium once again loses its stability in a super-critical Hopf bifurcation that gives rise to a stable limit cycle. Therefore, our system exhibits three limit cycles that surround the coexistence equilibrium. More precisely, a large-amplitude stable limit cycle encircles an unstable limit cycle, which, in turn, surrounds both the small-amplitude stable limit cycle and the coexistence equilibrium.

Small β implies a low mortality rate or a high birth rate for the specialist predator population. Fig. 4 shows that too high a birth rate or too low a death rate for the specialist predators makes the prey and the specialists vulnerable to perturbations that lead to extinction.

2.2.2. *Heteroclinic connection.* We can observe heteroclinic connections in two special situations. Fig. 5 shows a heteroclinic connection that joins a saddle equilibrium and a semi-stable equilibrium corresponding to a fold bifurcation. Increases in z pull down the prey null-cline, while maintaining a stable limit cycle (SLC) that surrounds a coexistence equilibrium. As we continue to increase z, the limit cycle collides with a saddle and a semi-stable equilibrium. As a result, two orbits form a cycle graph with the equilibria as the two vertices. One orbit coming out from a semi-stable equilibrium lies on the abscissa, and the other orbit emerges when the unstable manifold coming from the saddle equilibrium coincides with the stable manifold entering the semi-stable equilibrium. Finally, if we increase z further, the specialist predator population goes extinct for all initial conditions.

The second case to be discussed here is a heteroclinic connection that joins two saddle equilibria. We can think of this case as the one in Fig. 5(c), but we now vary β with fixed α, γ, δ, and z. Fig. 6(a) shows two basins of attractions separated by a separatrix (thick dot-dash curve), the stable manifold of the saddle point $E_{1,2}$. Trajectories below the separatrix approach the equilibrium where the prey and the specialists coexist, while trajectories above the separatrix sink to $E_{1,1}$ where specialists are extinct. Decreases in the parameter β slide the specialist predator null-cline to the left. Thus, as we decrease β, a super-critical Hopf bifurcation gives rise to a stable limit cycle that lies below the separatrix (Fig. 6(b)). This stable limit cycle enlarges, hits the separatrix, and vanishes in a heteroclinic orbit that connects two saddle equilibria (Fig. 6(c)). If we continue to decrease β, all trajectories are drawn towards stable equilibrium $E_{1,1}$ (Fig. 6(d)).

Fig. 5 tells us that the specialist predator population may go extinct if the generalist population grows. At high generalist density, increasing the birth rate or decreasing the mortality rate for the specialist predators can worsen the specialist's survival (Fig. 6).

2.3. **Two-parameter bifurcation diagram.** We have only discussed two particular phenomena in the previous section. Fig. 7 depicts the bifurcation curves that occur as we vary two parameters, z and β. This (β, z) parameter plane was obtained using the software package *XPPAUT* [11], which provides a simple interface to the continuation package *AUTO* [9].

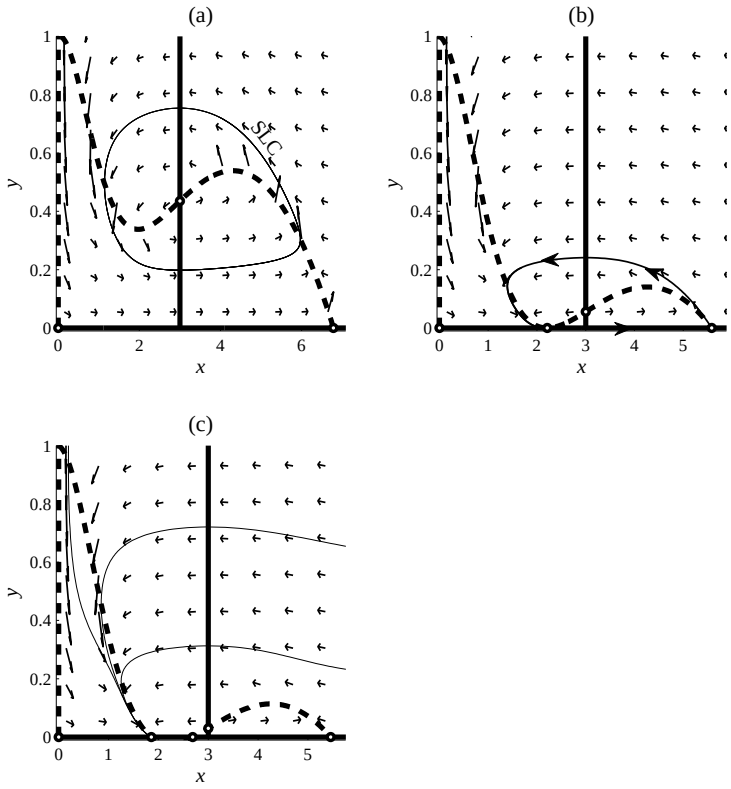

FIGURE 5. Phase portraits displaying vector fields and null-clines for system (9) with the parameter values $\alpha = 0.3$, $\gamma = 10$, $\delta = 1.65$, $\beta = 0.75$: (a) $z = 1.4$, (b) $z \approx 1.6249$, and (c) $z = 1.64$. Equilibria (circles) occur at the intersections of the prey null-clines (thin lines) and the predator null-clines (thick lines). As we increase z, a stable limit cycle (SLC) disappears in a heteroclinic connection that consists of two orbits: one orbit coming out from a semi-stable equilibrium lies on the abscissa, and the other orbit occurs when the unstable manifold coming from a saddle equilibrium coincides with the stable manifold entering the semi-stable equilibrium. Further increase in z leads all trajectories to approach the stable equilibrium, where the specialist predator goes extinct.

The (β, z) parameter plane is divided into regions $R(i, j)$ where $i(= 3, 4, 5)$ and $j(= 0, 1, 2, 3)$ indicate the number of equilibria in the first quadrant and the number of limit cycles that surround the coexistence equilibrium. Embedded figures are typical prey null-clines, $y = f(x)$, that are observed between dotted lines or thick dashed lines; in particular, the thick dashed lines represent branches of fold bifurcations.

Local bifurcations such as fold (thick dashed lines), transcritical (thin dot-dash curve), and sub-critical (thin curve) / super-critical (thick curve) Hopf bifurcations,

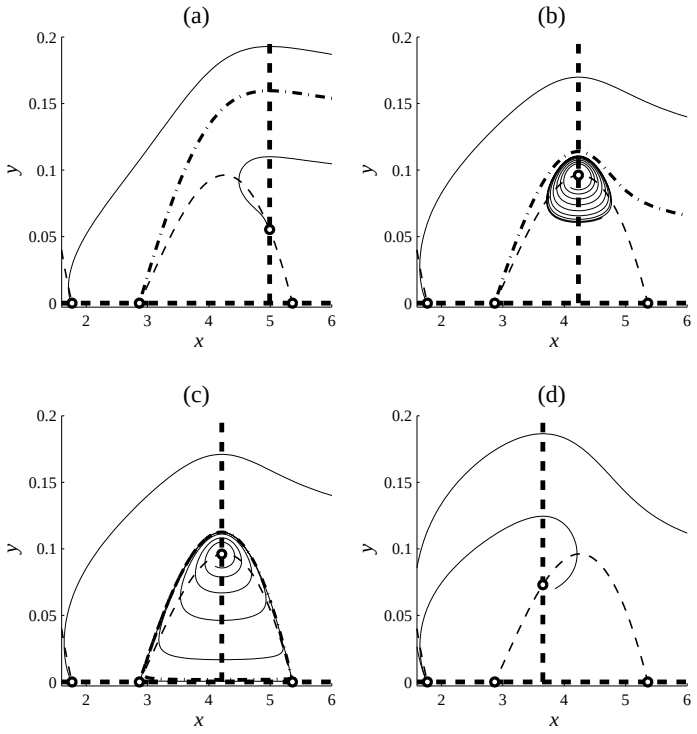

FIGURE 6. Phase portraits displaying vector fields and null-clines for system (9) with the parameter values $\alpha = 0.5$, $\gamma = 10$, $\delta = 1.65$, $z = 1.65$: (a) $\beta = 0.833$, (b) $\beta = 0.8088$, (c) $\beta \approx 0.8080363$, and (d) $\beta = 0.785$. Equilibria (circles) occur at the intersections of the prey null-clines (thin dashed lines) and the predator null-clines (thick dashed lines). As β decreases, (a) two basins of attractions are separated by a separatrix (dot-dash curve), and (b) unstable coexistence equilibrium E_2 is surrounded by a stable limit cycle after undergoing a super-critical Hopf bifurcation. As we continue to decrease β, (c) the stable limit cycle gets larger, hits the separatrix, and eventually disappears in a heteroclinic connection. Finally, (d) all trajectories approach the stable equilibrium, so that the specialist predator goes extinct.

can be found by analyzing local dynamics in the neighborhood of an equilibrium. If a limit cycle appears without a change in the stability of an equilibrium, we should consider a global bifurcation. Fig. 7 shows a branch of global cyclic-fold bifurcations (thick dot-dash curves) at which stable and unstable limit cycles appear and separate or coalesce and disappear. We also observe two branches of heteroclinic orbits indicated by H: in the enlarged subfigure inside Fig. 7, a branch of heteroclinic orbits connecting saddle and a semi-stable equilibrium is drawn as cross marks ($\times$) to distinguish a branch of heteroclinic orbits that link two saddle equilibria (thin dashed curve).

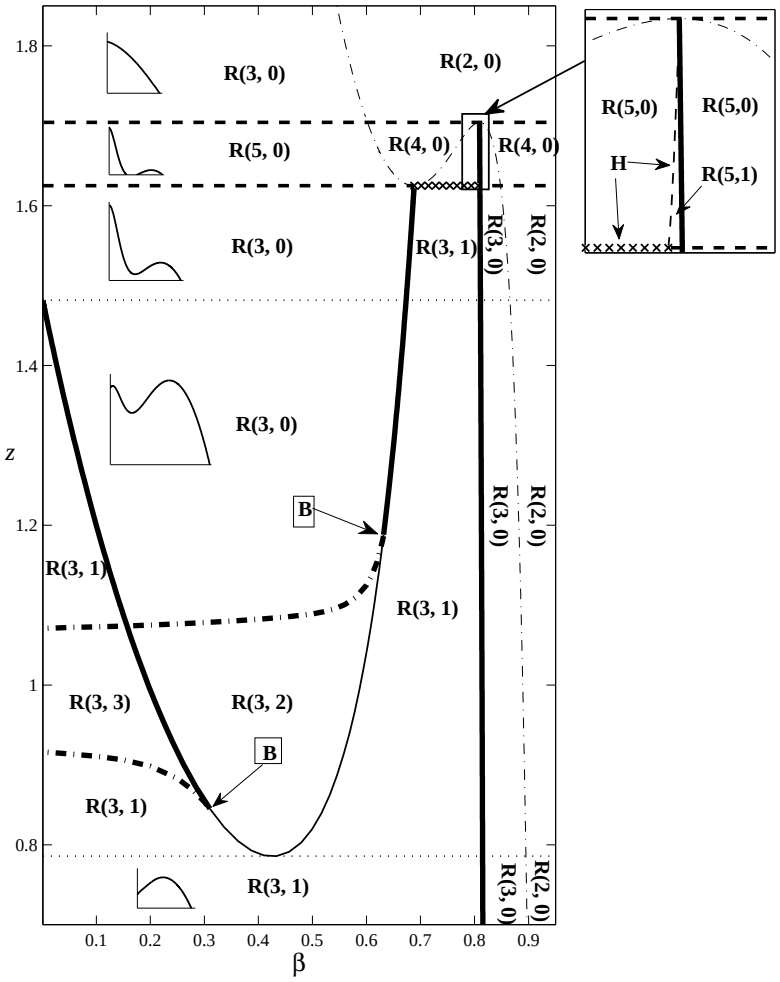

FIGURE 7. The (β, z) parameter plane for laissez-faire model (9) with $\alpha = 0.5$, $\delta = 1.65$, and $\gamma = 10$. The parameter plane is divided into regions $R(i, j)$ where $i(= 3, 4, 5)$ and $j(= 0, 1, 2, 3)$ indicate the number of equilibria shown in the first quadrant and the number of limit cycles that surround the coexistence equilibrium. Embedded subplots are typical prey null-clines, $y = f(x)$, observed in each region bounded by dotted lines or thick dashed lines. The thick dashed lines, in particular, represent branches of fold bifurcations. The system also exhibits transcritical (thin dot-dash curve), super-critical Hopf (thick solid curve), sub-critical Hopf (thin solid curve), and global cyclic-fold (thick dot-dash curve) bifurcations. Curves of heteroclinic connections are indicated by H. At a codimension-two Bautin bifurcation (B), a Hopf bifurcation changes from super- to sub-critical and from the Bautin bifurcation, a curve of cyclic-fold emanates. A pitchfork bifurcation (PFB) can be found at the intersections of curves of fold, transcritical, and super-critical Hopf bifurcations and a branch of heteroclinic connections.

The codimension of a bifurcation is the number of parameters that must be varied for the bifurcation to occur. For example, a fold bifurcation is a codimension-one bifurcation since it can be achieved by changing a single parameter. We observe a bifurcation point where a Hopf bifurcation changes from super- to sub-critical. From this point, a curve of cyclic-fold bifurcations also emanates. This codimension-two bifurcation is called a Bautin (B) or generalized Hopf bifurcation [26].

Here is one example of how to study dynamical behaviors as we change a bifurcation parameter. Let us take the transect $z = 1$ in Fig. 7 and let us vary β between 0.01 and 0.95 for fixed $\alpha(= 2)$, $\gamma(= 10)$, $\delta(= 1.65)$, and $z(= 1)$. Recall that increasing (decreasing) β leads to the rightward (leftward) movement of the specialist-predator vertical null-cline, and varying β can give rise to a local Hopf bifurcation. When the x-coordinate of a coexistence equilibrium, x^*, is less than $\hat{k} = k_1$, there are three equilibria, E_0, $E_{1,1}$, and E_2, in the first quadrant. For $x^* > k_1$, $E_{1,1}$ changes from an unstable saddle to a stable node and no coexistence equilibrium E_2 occurs in the interior of the first quadrant. We have a transcritical bifurcation (thin dot-dash curve) since $E_{1,1}$ and E_2 exchange stability.

The second component of $R(i, j)$ in Fig. 7 denotes the number of limit cycles. For small β, the predator vertical null-cline is positioned on the left side of the left hump of the prey null-cline $y = f(x)$. Our system exhibits three limit cycles that surround a coexistence equilibrium. As we increase β, the coexistence equilibrium undergoes a reverse super-critical Hopf bifurcation (thick solid curve) that destroys the stable, small-amplitude limit cycle. As we continue to increase β, the coexistence equilibrium loses its stability and an unstable limit cycle disappears in a sub-critical Hopf bifurcation. If we increase β further, the coexistence equilibrium regains stability and the remaining stable limit cycle is annihilated in a reverse (super-critical) Hopf bifurcation.

As a prelude to our discussion for the time-dependent parameter $z(t)$ in the next section, we will consider some bifurcation diagrams for the time-independent parameter z in regions of interest.

2.3.1. *Bifurcation diagrams in z for the occurrence of multiple limit cycles.* Fig. 8 depicts the bifurcation diagram for z in the region where multiple limit cycles occur. The thick and thin lines indicate the x-coordinates of stable and unstable coexistence equilibria. For small z, the coexistence equilibrium is unstable, but it becomes stable after undergoing either a reverse super-critical (HB^+) or sub-critical (HB^-) Hopf bifurcation as we increase z. Changing z also changes the number of global cyclic-fold bifurcations (CFB) at which stable and unstable limit cycles coalesce and disappear.

The series of subplots shows, from top to bottom, how the bifurcation diagram for z changes as we increase β around the codimension-two Bautin bifurcation. Increasing β causes a super-critical Hopf bifurcation to occur near a global cyclic-fold bifurcation. As we continue to increase β, the super-critical Hopf bifurcation and the adjacent cyclic-fold bifurcation eventually collide and disappear, so that a sub-critical Hopf bifurcation arises in a Bautin bifurcation.

2.3.2. *Bifurcation diagrams for z as it crosses two branches of fold bifurcations.* We illustrate a sequence of bifurcation diagrams for z in Figs. 9–12 to show how pitchfork bifurcations and heteroclinic connections occur with increasing β and fixed $\alpha(= 0.5)$, $\gamma(= 10)$, and $\delta(= 1.65)$. Recall that the x-coordinates of coexistence equilibria only depend on β, so that the branch of coexistence equilibria comes to

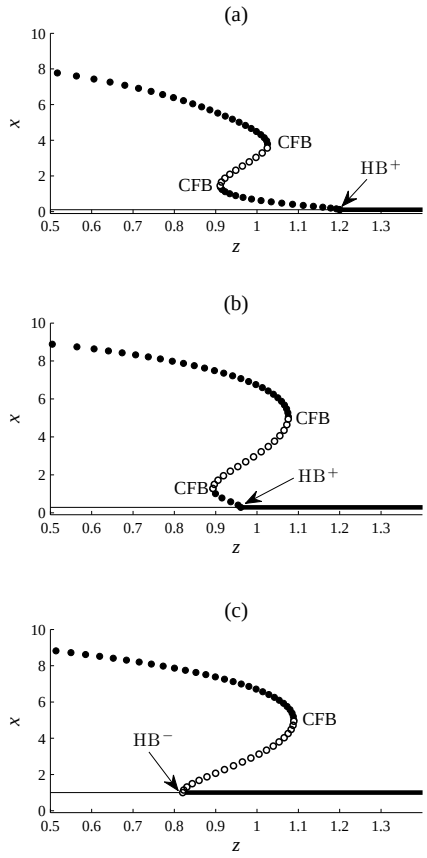

FIGURE 8. Bifurcation diagrams for laissez-faire model (9). The maximum values of the x-coordinates of stable limit cycles and unstable limit cycles are drawn as filled and open circles. Stable coexistence equilibria (thick solid line) and unstable coexistence equilibria (thin solid line) are computed for increasing z with (a) $\beta = 0.1$, (b) $\beta = 0.22$, and (c) $\beta = 0.5$: $\alpha = 0.5$, $\gamma = 10$, $\delta = 1.65$. (a) and (b) Two global cyclic-fold bifurcations (CFB) and one local reverse super-critical Hopf (HB^+) occur as we increase z. (c) One reverse sub-critical Hopf bifurcation (HB^-) and one cyclic-fold bifurcation appear as we increase z.

be horizontal. Also, the coexistence equilibrium does not exist in the interior of the first quadrant if it is a saddle point.

As we increase β, in Fig. 9, the branch of coexistence equilibria rises, sweeping through the lower branch of the equilibria where the specialists go extinct. Meanwhile, we observe an exchange of stability between the coexistence equilibrium and the equilibrium where only the prey survive. If we continue to increase β, a reverse super-critical Hopf bifurcation (HB) occurs in the bifurcation parameter range of interest. The Hopf bifurcation slides rightwards and eventually it hits a pitchfork

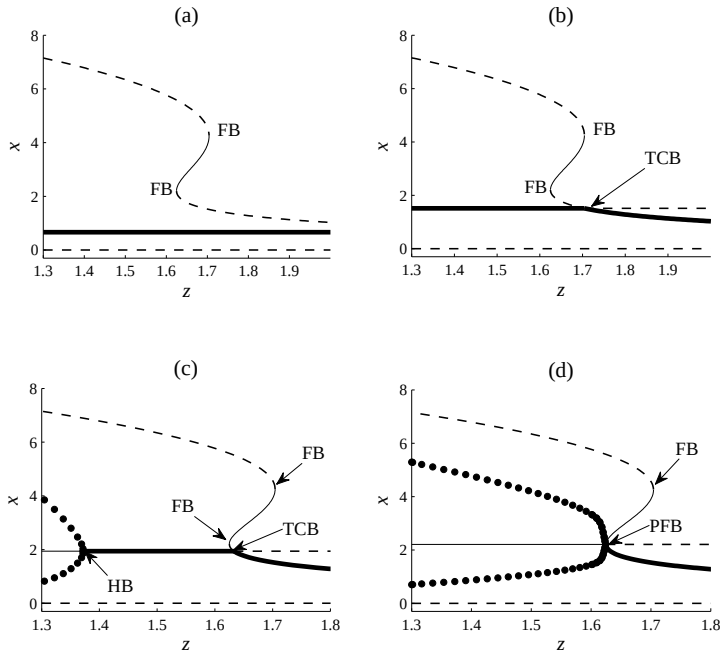

FIGURE 9. Bifurcation diagrams for z across two branches of fold bifurcations in laissez-faire model (9) with different values of β and fixed $\alpha = 0.5$, $\gamma = 10$, and $\delta = 1.65$: (a) $\beta = 0.4$, (b) $\beta \approx 0.6018$, (c) $\beta = 0.66$, and (d) $\beta \approx 0.6882$. The highest and lowest values of x-coordinates of stable limit cycles (filled circles) and the x-coordinates of unstable node/focus (thin solid curve), stable node/focus (thick solid curve), and saddle (dashed curve) equilibria are computed as we vary z. FB: fold bifurcation, TCB: transcritical bifurcation, PFB: pitchfork bifurcation, and HB: (super-critical) Hopf bifurcation. When the coexistence equilibrium is saddle point, it exists in the fourth quadrant.

bifurcation (PFB) at which a transcritical and a fold bifurcation collide with each other. Please note that the pitchfork bifurcation cannot be classified as either super- or sub-critical. The classification of sub- and super-critical pitchfork bifurcations may be impossible when we have equations in addition to a single one-dimensional differential equation [40].

As we continue to increase β after the collision of branches of fold, transcritical, and Hopf bifurcations, the system exhibits a heteroclinic connection (H) at which a stable limit cycle terminates as shown in Figs. 10 and 11. Outside subfigures display the prey and predator null-clines for each bifurcation point. These two bifurcation diagrams correspond to the two cases of heteroclinic connections described in section 2.2.2.

Further increases in β cause both a heteroclinic connection (H) and a transcritical bifurcation (TCB) to approach fold bifurcation FB_2 in Fig. 12. When a transcritical

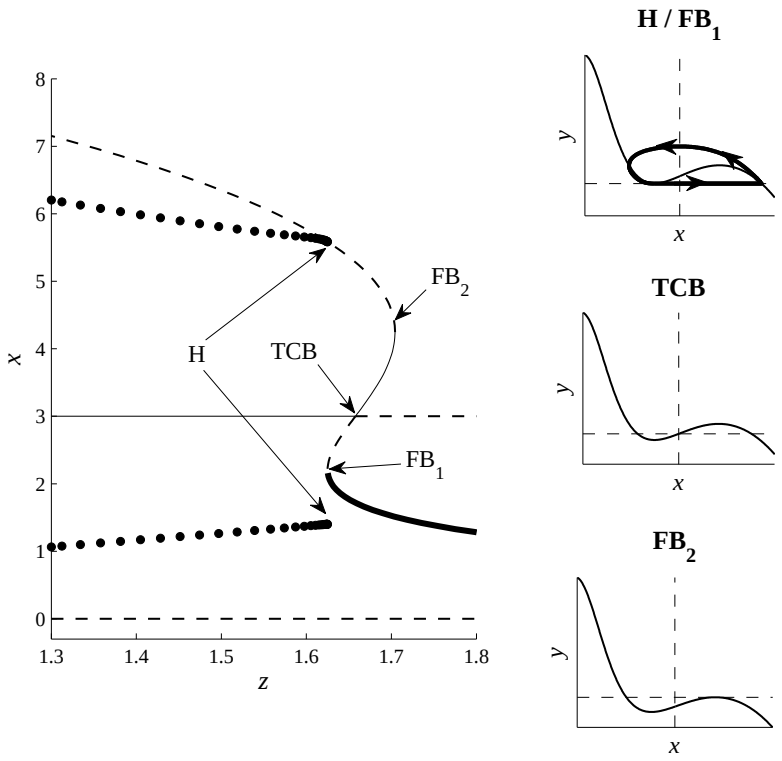

FIGURE 10. Bifurcation diagrams for z around a heteroclinic connection in laissez-faire model (9). The highest and lowest values of the x-coordinates of stable limit cycles (filled circle) and the x-coordinates of stable node/focus (thick solid curve), unstable node/focus (thin solid curve), and saddle (dashed curve) equilibria are computed with $\alpha = 0.5$, $\beta = 0.75$, $\gamma = 10$, and $\delta = 1.65$. As we increase z, a heteroclinic orbit (H) occurs by connecting a saddle equilibrium and a semi-stable equilibrium that corresponds to a fold bifurcation (FB_1). If we continue to increase z, the system exhibits a transcritical (TCB) and a fold (FB_2) bifurcation. Outside subplots illustrate the predator null-clines (dashed line) and the prey null-clines (solid line) that appear at each bifurcation point.

bifurcation collides with the fold bifurcation, we can see a pitchfork bifurcation at which a heteroclinic connection vanishes. As the branch of coexistence equilibria rises, a reverse (super-critical) Hopf bifurcation (HB) slides to the left rapidly and a fold and a transcritical bifurcation appear through the upper branch of specialist-predator extinction equilibria.

3. **Laissez-faire model with slowly varying $z(t) = z_0 + M\sin(\epsilon t)$.** In this section, we consider laissez-faire model (9) with slowly varying $z(t) = z_0 + M\sin(\epsilon t)$ where z_0, M, and ϵ ($\ll 1$) are positive. System (9) with time-dependent parameter

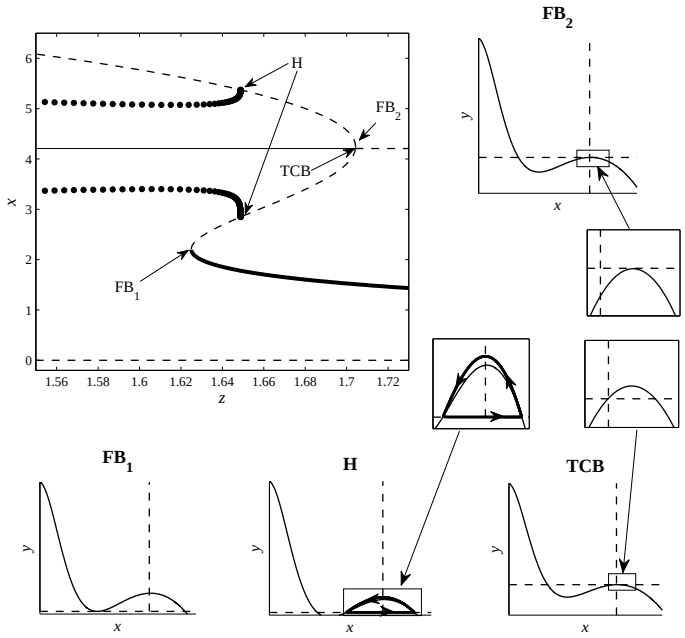

FIGURE 11. Bifurcation diagram for z around a heteroclinic orbit in laissez-faire model (9) with $\alpha = 0.5$, $\beta = 0.808$, $\gamma = 10$, and $\delta = 1.65$. The system possesses a heteroclinic orbit that connects two saddle equilibria with increasing z. H stands for a heteroclinic connection, $\mathrm{FB}_{1,2}$ for a fold bifurcation, and TCB for a transcritical bifurcation. Filled circles are the highest and lowest values of x-coordinates of stable limit cycles, thick and thin solid curves indicate the x-coordinates of stable and unstable node/focus equilibria, and dashed curves denote the x-coordinates of saddle equilibria. In outside subplots, solid and dashed curves indicate the prey and predator null-clines.

$z(t)$ can be written as a fast-slow system,

$$\frac{dx}{dt} = x\left(1 - \frac{x}{\gamma}\right) - \frac{x}{1+x}\, y - \frac{\delta x^2}{\delta^2 + x^2}\, z, \tag{32a}$$

$$\frac{dy}{dt} = \alpha y \left(\frac{x}{1+x} - \beta\right), \tag{32b}$$

$$\frac{dz}{dt} = \epsilon M \cos(\epsilon t). \tag{32c}$$

In order to analyze fast-slow system (32), we will employ the method of *dissection* pioneered by Rinzel [38, 45]: Rinaldi and Scheffer [37] also described how to study fast and slow processes in ecosystems. The fast variables, $x(t)$ and $y(t)$, reach a steady state rapidly while slow variable $z(t)$ does not change significantly. Thus, the dynamics of fast variables can be studied assuming that $dz/dt = 0$, which is equivalent to treating z as a time-independent parameter. In sections 2.2 and 2.3,

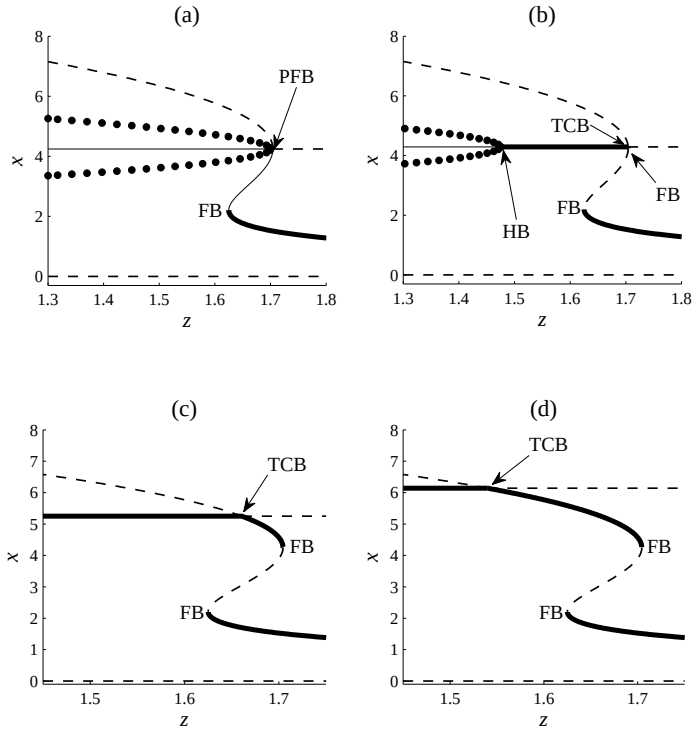

FIGURE 12. Bifurcation diagrams for z across branches of two fold bifurcations with fixed $\alpha = 0.5$, $\gamma = 10$, and $\delta = 1.65$ for different values of β: (a) $\beta \approx 0.80935$, (b) $\beta = 0.811$, (c) $\beta = 0.84$, and (d) $\beta = 0.86$. The highest and lowest values of x-coordinates of stable limit cycles (filled circle) and the x-coordinates of unstable node/focus equilibria (thin solid curve), stable node/focus equilibria (thick solid curve), and saddle equilibrium points (dashed curve) are computed as we vary z. FB: fold bifurcation, TCB: transcritical bifurcation, PFB: pitchfork bifurcation, and HB: (super-critical) Hopf bifurcation. Note that the saddle coexistence equilibrium does not appear in the interior of the first quadrant.

we numerically analyzed the dynamics of fast subsystem (32a, b) treating z as a bifurcation parameter. We will now slowly vary a sinusoidal function $z(t)$ in time, crossing over a range where the fast subsystem tracks its stable attractors. During the slow variation in $z(t)$, system (32) undergoes successive alternations between repetitive spiking oscillations (active phase) and a quasi-steady state (silent phase). This phenomenon is called bursting.

Bursting has been rigorously studied in neural models [19, 21, 22, 45]. In contrast, few ecologists have studied bursting (but see, for instance, [37, 44]). Many authors have analyzed periodically forced predator–prey models, emphasizing chaotic aspects [1, 10, 20, 25, 29, 33, 35, 36, 39]. Unlike those chaos papers, we will show how bursting occurs in our fast-slow system.

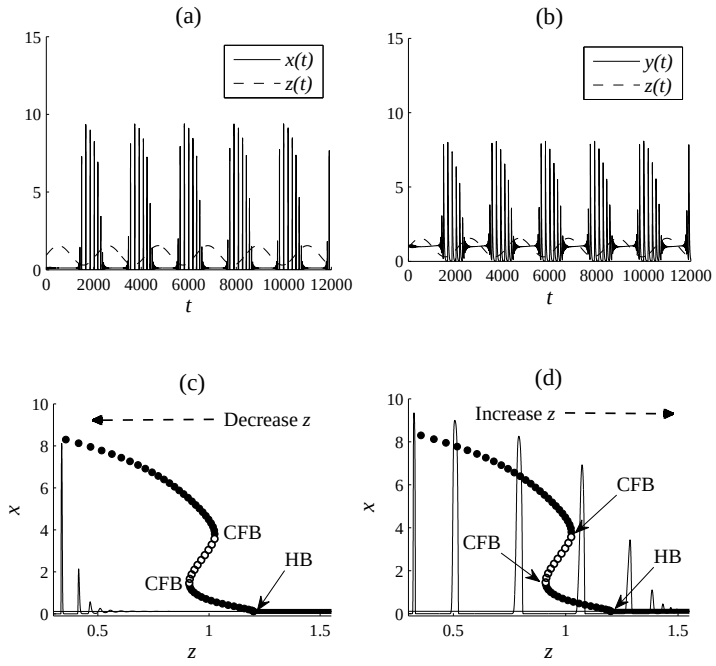

FIGURE 13. Bursting induced by a periodic modulation of the control parameter $z(t)$ between 0.3 and 1.55 in system (32) for $\alpha = 0.5$, $\beta = 0.1$, $\gamma = 10$, $\delta = 1.65$, $M = 0.625$, and $\epsilon = 0.003$ with initial conditions $(x_0, y_0, z_0) = (0.1111, 0.9833, 0.925)$. The time series of (a) the prey $(x(t))$ population and (b) specialist predator $(y(t))$ population are illustrated with the time series of the generalist predator $(z(t))$ populations. A trajectory of $x(t)$ for one period of time in the generalist predator $z(t)$ is superimposed on the bifurcation diagram for the time-independent parameter z as we (c) decrease $z(t)$ or (d) increase $z(t)$. HB signifies a (super-critical) Hopf bifurcation and CFB denotes a cyclic-fold bifurcation. In the bifurcation diagram for the bifurcation parameter z, thin and thick lines indicate the x-coordinates of unstable and stable equilibria. Filled and open circles represent the highest values of the x-coordinates of stable and unstable limit cycles.

We numerically solved our fast-slow system using the *XPPAUT* ODE integrator, Stiff, that is based on the stiff algorithm in [34]. *XPPAUT* also has other adaptive integrators such as Gear [12], Rosenbrock [34], and CVODE [8] that are implicit and work well for stiff problems.

In order to make model (32) burst, it is usually assumed that the fast and slow variables have considerably different time scales. Choosing ϵ $(= 0.003)$ small enough, we can observe (periodic) bursting while we slowly change slow variable $z(t)$, $0.3 \leq z \leq 1.55$, between quiescent (bifurcation of equilibria) and spiking (bifurcation of limit cycles) regimes periodically (Fig. 13(a) and (b)): a periodic bursting occurs

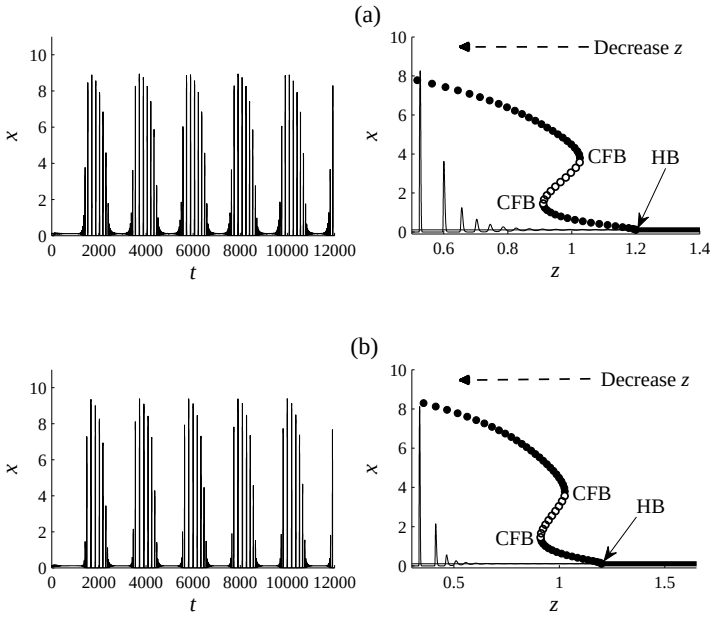

FIGURE 14. Time series of $x(t)$ and the corresponding bifurcation diagrams for the time-independent parameter z that describe the slow passage through a Hopf bifurcation (HB) in system (32): (a) $0.5 \leq z \leq 1.4$ and (b) $0.3 \leq z \leq 1.55$ with $\alpha = 0.5$, $\beta = 0.1$, $\gamma = 10$, $\delta = 1.65$, $\epsilon = 0.003$, and different values of M, (a) $M = 0.45$ and (b) $M = 0.625$. Applied initial conditions are (a) $(x_0, y_0, z_0) = (0.1111, 0.9945, 0.95)$ and (b) $(x_0, y_0, z_0) = (0.1111, 0.9833, 0.925)$. In the bifurcation diagram for the bifurcation parameter z, thin and thick lines indicate the x-coordinates of unstable and stable equilibria. Filled and open circles represent the highest values of the x-coordinates of stable and unstable limit cycles. A trajectory of $x(t)$ for one period of $z(t)$ is superimposed in the bifurcation diagram for time-independent parameter z. HB: a (super-critical) Hopf bifurcation and CFB: a cyclic-fold bifurcation.

conditionally because it exists for certain parameter values. This case is when we change z between 0.3 and 1.55 with $\beta = 0.1$ in the (β, z) parameter plane (Fig. 7), crossing a branch of super-critical Hopf bifurcations and two branches of cyclic-fold bifurcations (Fig. 13(c), (d)).

The reader may question why the trajectory in Fig. 13(c) does not diverge immediately from the state corresponding to the unstable equilibrium in a reverse super-critical Hopf bifurcation (HB). The feature highlighted in Fig. 14 is the slow passage through a Hopf bifurcation [3, 16, 21], where the transition from resting state to spiking state is delayed due to the memory of the previous state. By increasing the amplitude of the forcing $z(t)$, the delay is prolonged because the longer the system stays at the resting state corresponding to the stable equilibrium, the longer it takes to diverge from the equilibrium.

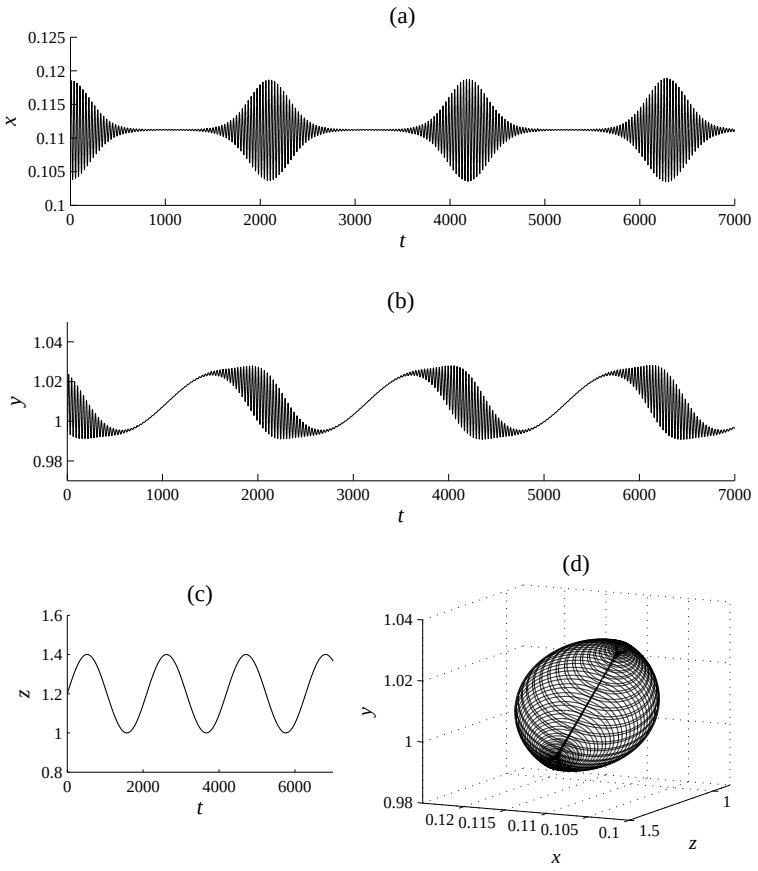

FIGURE 15. Time series of (a) $x(t)$ and (b) $y(t)$ that describe SuperHopf/Cyclic-fold bursting where $1 \leq z \leq 1.4$ (see (c) for the time series of $z(t)$) in system (32) with $\alpha = 0.5$, $\beta = 0.1$, $\gamma = 10$, $\delta = 1.65$, $\epsilon = 0.003$, and $M = 0.2$. Initial conditions are $x_0 = 0.1111$, $y_0 = 0.9945$, and $z_0 = 1.2$. (d) A bursting trajectory in three-dimensional phase space (z, x, y).

Izhikevich [22] identified 120 different types of bursting and described their topological features. Assuming that the system is initially at rest and starts spiking, he named bursters according to the types of bifurcations of equilibrium and limit cycle attractors. For example, for subHopf/cyclic-fold bursting a resting state disappears in a sub-critical Hopf bifurcation and a spiking state is terminated in a cyclic-fold bifurcation. The reader may refer to [19, 21, 22] for more information.

Rather than showing all possible types of bursting, we will discuss some bursting phenomena that occur in system (32). Again, we usually assume that the system is initially at quasi-steady state.

3.1. **SuperHopf/Cyclic-fold.** Fig. 15(a) and (b) display SuperHopf/cyclic-fold bursting where $1 \leq z(t) \leq 1.4$ (Fig. 15(c)) with $\alpha = 0.5$, $\beta = 0.1$, $\gamma = 10$, $\delta = 1.65$,

$\epsilon = 0.003$, and $M = 0.2$. Referring to the (β, z) parameter plane in Fig. 7, we see that the fast subsystem undergoes super-critical Hopf and cyclic-fold bifurcations. That is, slow modulation of $z(t)$ between 1 and 1.4 causes the fast subsystem to trigger spiking and to terminate the repetitive spiking in a super-critical Hopf bifurcation. The corresponding phase portrait is depicted in Fig. 15(d).

3.2. **SubHopf/Cyclic-fold.** SubHopf/Cyclic-fold bursting, shown in Fig. 16(a) and (b), arises when the resting state loses stability via a sub-critical Hopf bifurcation (HB) and the repetitive firing state vanishes through a cyclic-fold bifurcation (CFB). This kind of bursting is called elliptic by Rinzel [38] due to an elliptic shape of the profile of oscillations; however, many subHopf/cyclic-fold bursters do not have elliptic profiles, so the use of the term elliptic bursting should be avoided [22].

As we decrease $z(t)$, the fast subsystem exhibits the delayed loss of stability through a sub-critical Hopf bifurcation (Fig. 16(c)). When $z(t)$ starts to increase, the trajectory for fast variable $x(t)$ finally jumps to the stable limit cycle and falls to the resting state corresponding to a stable equilibrium via a cyclic-fold bifurcation (Fig. 16(d)). Unlike the three-dimensional phase portrait in Fig. 15(d) that illustrate all solutions over $0 \leq t \leq 15000$, Fig. 16(e) shows a phase portrait for one period of $z(t)$, so that we can see the transition between a quiescent and a active phase while we slowly decrease and increase $z(t)$. Starting from the point indicated by a star ($\star$), the trajectory flows backward with a decrease in $z(t)$, starts to oscillate, tracking the stable, large-amplitude limit cycle, and eventually falls to the resting state that corresponds to a stable equilibrium via a cyclic-fold bifurcation.

3.3. **Bursting across a heteroclinic connection.** In Fig. 17, with $\beta = 0.75$, we let z vary between 1.4 and 1.68, so that our system passes through a transcritical bifurcation and a heteroclinic connection associated with a fold bifurcation. A transcritical bifurcation has, in fact, no effect on transition between a resting state and a repetitive spiking state. A jump either from the resting state to a stable limit cycle or from the stable limit cycle to the resting state occurs via the fold bifurcation. When we slowly decrease z with time, a trajectory jumps to the upper branch of saddle equilibria through an unstable manifold that emanates from a semi-stable equilibrium corresponding to a fold bifurcation (Fig. 17(c)). As we then increase z, the trajectory that has tracked the upper branch of saddle equilibria now leaves this branch and begins to oscillate (Fig. 17(d)).

4. **Discussion.** In this paper, we carried out analytical and numerical studies for a laissez-faire model with two predators, specialists and generalists. Treating the generalist predator population as a bifurcation parameter, we highlighted two features, the existence of multiple (up to three) limit cycles and heteroclinic connections. As shown in the (β, z) parameter plane, the laissez-faire model with a time-independent constant generalist predator population exhibits rich dynamics including fold, transcritical, Hopf, and cyclic-fold bifurcations. In addition, the system possesses a codimension-two Bautin bifurcation at which a Hopf bifurcation changes from super- to sub-critical and from which a curve of cyclic-fold bifurcations emanates. We also observed a pitchfork bifurcation at which branches of transcritical, fold, and super-critical Hopf bifurcations collide with a branch of heteroclinic connections.

Our numerical studies showed that when the generalist predator population is low, increasing the birth rate or decreasing the mortality rate for the specialist

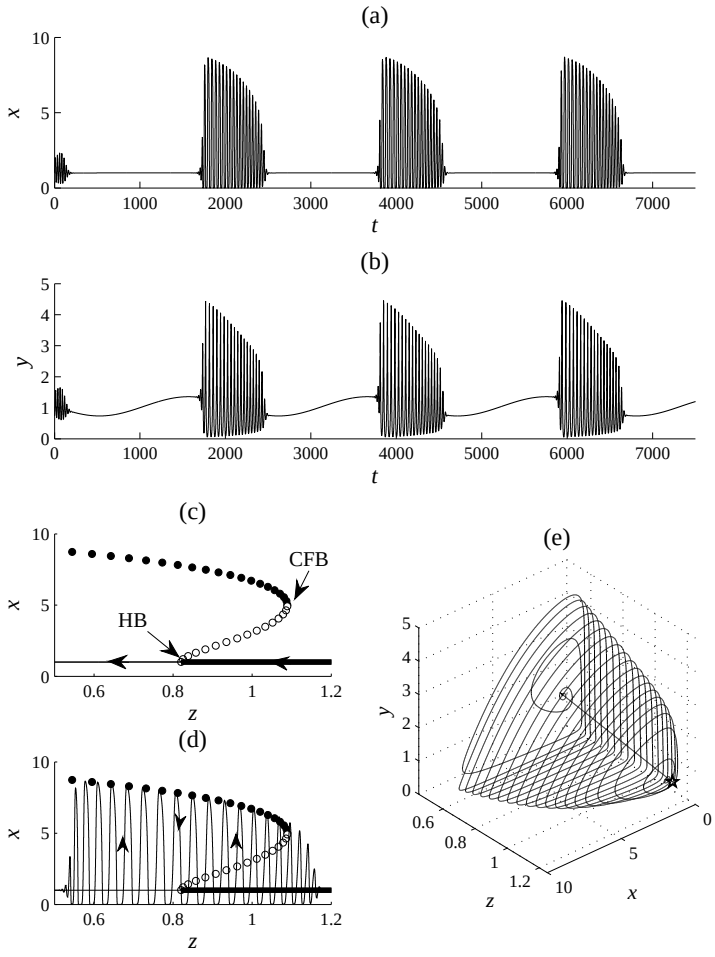

FIGURE 16. Time series of (a) $x(t)$ and (b) $y(t)$ that illustrate SubHopf/Cyclic-fold bursting where $0.5 \leq z \leq 1.2$ in system (32) with $\alpha = 0.5$, $\beta = 0.5$, $\gamma = 10$, $\delta = 1.65$, $\epsilon = 0.003$, and $M = 0.35$. Initial conditions for each variable are $(x_0, y_0, z_0) = (1, 0.7362, 0.85)$. In (c) and (d), a trajectory of $x(t)$ in half period of $z(t)$ is superimposed in the bifurcation diagram for the time-independent parameter z: HB stands for a sub-critical Hopf bifurcation and CFB for a cyclic-fold bifurcation. Arrows indicate the direction of the movement of the trajectories with increasing time. (e) Three-dimensional phase space (z, x, y) is pictured in one period of $z(t)$. A star indicates a point where $z(t) = 1.2$.

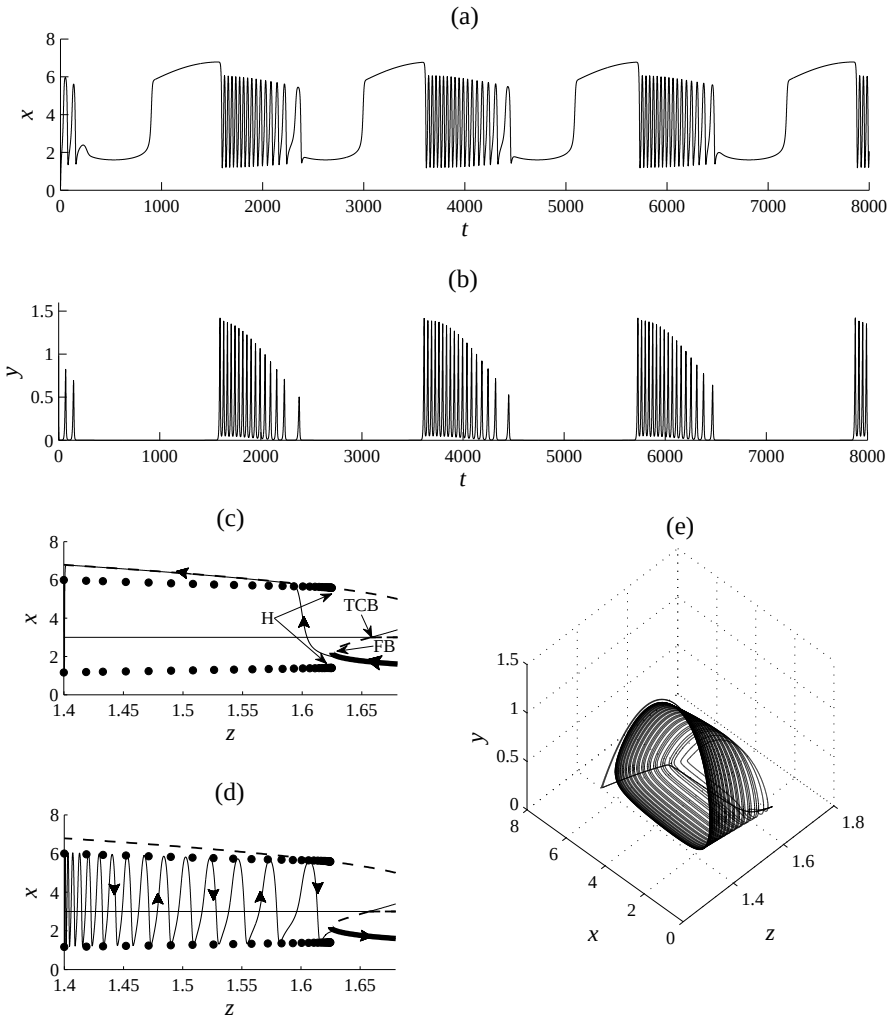

FIGURE 17. Time series of (a) $x(t)$ and (b) $y(t)$ that depict bursting where $1.4 \leq z \leq 1.68$ with $\alpha = 0.5$, $\beta = 0.75$, $\gamma = 10$, $\delta = 1.65$, $\epsilon = 0.003$, and $M = 0.14$: initial conditions are $(x_0, y_0, z_0) = (0.11, 0.983, 1.54)$. In (c) and (d), a trajectory of $x(t)$ in half period of $z(t)$ is superimposed in the bifurcation diagram for the time-independent parameter z: TCB stands for a transcritical bifurcation, FB for a fold bifurcation, and H for a heteroclinic connection. The x-coordinates of stable node/focus (thick solid curve), unstable node/focus (thin solid curve), and saddle (dashed curve) equilibria are computed. Filled circles are the highest and lowest values of the x-coordinates of stable limit cycles. Arrows indicate the direction of the movement of the trajectories with increasing time. (e) illustrates a three-dimensional phase portrait.

predator population tends to induce population cycles. However, when the generalist predator population thrives, the population cycles are less likely to occur, so that the prey and specialist-predator dynamics becomes stabilized. Thus, our laissez-faire model supports the hypothesis that the generalist predator population has a stabilizing effect on a population cycle driven by the specialist predator population [13].

The rates of processes in an ecosystem are often very different. By forcing the generalist predator population to slowly vary with time, we analyzed how a fast subsystem that governs the prey and specialist-predator dynamics responds to the slow variation in the generalist predator population.

By the method of dissection, bursting phenomenon, successive alternations between repetitive spiking oscillations and a silent phase, was driven by a slow change in the generalist predator number that marches our system through bifurcations of the fast subsystem. While the periodically forced laissez-faire system underwent a Hopf bifurcation, we found the delayed loss of stability due to the slow slow passage through the Hopf bifurcation. This delay or memory effect was prolonged as the amplitude of the fluctuations in the generalist predator population gets larger. Thus, if the generalist predator population fluctuates substantially, the prey and specialist-predator dynamics is stabilized after all. However, this memory effect may not be observable empirically since the delay can be shortened or reversed by weak noise [21].

We have observed (periodic) bursting with small ϵ ($= 0.003$). However, periodic bursting will not always occur, no matter how small we make ϵ. It is important to remember that we forced our system to undergo bifurcations by choosing appropriate parameter values. In addition, our system can also exhibit quasi-periodic and even chaotic bursting. There are many studies in neuroscience considering chaotic dynamics in connection with bursting and beating (continuous spiking). The interested reader may refer to [4, 6, 7, 27, 31, 42].

Acknowledgments. The first author would like to thank Professor Shea-Brown for his helpful comments and suggestions.

REFERENCES

[1] J. C. Allen, *Chaos and phase-locking in predator–prey models in relation to functional response*, Fla. Entomol., **73** (1990), 100–110.

[2] M. Andersson and S. Erlinge, *Influence of predation on rodent populations*, Oikos, **29** (1977), 591–597.

[3] S. M. Baer, T. Erneux and J. Rinzel, *The slow passage through a Hopf bifurcation: Delay, memeory effect, and resonance*, SIAM J. Appl. Math., **49** (1989), 55–71.

[4] C. C. Canavier, J. W. Clark and J. H. Byrne, *Routes to chaos in a model of a bursting neuron*, Biophys. J., **57** (1990), 1245–1251.

[5] G. Caughley and J. H. Lawton, *Plant-herbivore systems*, in "Theoretical Ecology: Principles and Applications" (eds. R. M. May), Blackwell, Oxford, (1981), 132–166.

[6] T. R. Chay, Y. S. Fan and Y. S. Lee, *Bursting, spiking, chaos, fractals, and universality in biological rhythms*, Int. J. Bifurcat. Chaos, **5** (1995), 595–635.

[7] T. R. Chay and J. Rinzel, *Bursting, beating, and chaos in an excitable membrane model*, Biophys. J., **47** (1985), 357–366.

[8] S. D. Cohen and A. C. Hindmarsh, *CVODE, a stiff/nonstiff ODE solver in C*, Comput. Phys., **10** (1996), 138–143.

[9] E. Doedel, A. R. Champneys, T. Fairgrieve, Y. Kuznetsov, B. Oldeman, R. Paffenroth, B. Sandstede, X. Wang and C. Zhang, "AUTO-07P: Continuation and Bifurcation Software for Ordinary Differential Equations," Technical report, Concordia University, Montreal, Canada, 2006.

[10] F. Doveri, Y. Kuznetsov, S. Muratori, S. Rinaldi and M. Scheffer, *Seasonality and chaos in a plankton–fish model*, Theor. Popul. Biol., **43** (1992), 159–183.
[11] B. Ermentrout, "Simulating, Analyzing, and Animating Dynamical Systems: A Guide to XPPAUT for Researchers and Students," SIAM, Philadelphia, 2002.
[12] C. W. Gear, *The numerical integration of ordinary differential equations*, Math. Comp., **21** (1967), 146–156.
[13] I. Hanski, L. Hansson and H. Henttonen, *Specialist predators, generalist predators and the microtine rodent cycle*, J. Anim. Ecol., **60** (1991), 353–367.
[14] I. Hanski, H. Henttonen, E. Korpimäki, L. Oksanen and P. Turchin, *Small-rodent dynamics and predation*, Ecology, **82** (2001), 1505–1520.
[15] G. W. Harrison, *Global stability of predator–prey interactions*, J. Math. Biol., **8** (1979), 159–171.
[16] L. Holden and T. Erneux, *Slow passage through a Hopf bifurcation: from oscillatory to steady state solutions*, SIAM J. Appl. Math., **53** (1993), 1045–1058.
[17] C. S. Holling, *The components of predation as revealed by a study of small mammal predation of the European pine sawfly*, Can. Entomol., **91** (1959), 293–320.
[18] C. S. Holling, *Some characteristics of simple types of predation and parasitism*, Can. Entomol., **91** (1959), 385–398.
[19] F. C. Hoppensteadt and E. M. Izhikevich, "Weakly Connected Neural Networks," Springer-Verlag, New York, 1997.
[20] M. Inoue and H. Kamifukumoto, *Scenarios leading to chaos in a forced Lotka–Volterra model*, Prog. Theor. Phys., **71** (1984), 930–937.
[21] E. M. Izhikevich, "Dynamical Systems in Neurosciences: The Geometry of Excitability and Bursting," MIT Press, Cambridge, 2007.
[22] E. M. Izhikevich, *Neural excitability, spiking, and bursting*, Int. J. Bifurcat. Chaos, **10** (2000), 1171–1266.
[23] T. Klemola, M. Tanhuanpää, E. Korpimäki and K. Ruohomäki, *Specialist and generalist natural enemies as an explanation for geographical gradients in population cycles of northern herbivores*, Oikos, **99** (2002), 83–94.
[24] E. Korpimäki, L. Oksanen, T. Oksanen, T. Klemola, K. Norrdahl and P. B. Banks, *Vole cycles and predation in temperate and boreal zones of Europe*, J. Anim. Ecol., **74** (2005), 1150–1159.
[25] M. Kot, G. S. Sayler and T. W. Schultz, *Complex dynamics in a model microbial system*, Bull. Math. Biol., **54** (1992), 619–648.
[26] Y. A. Kuznetsov, "Elements of Applied Bifurcation Theory," Springer-Verlag, New York, 2004.
[27] P. Lebrun and I. Atwater, *Chaotic and irregular bursting electrical activity in mouse pancreatic B-cells*, Biophys. J., **48** (1985), 529–531.
[28] P. H. Leslie, *Some further notes on the use of matrices in population mathematics*, Biometrika, **35** (1948), 213–245.
[29] R. W. Leven, B. P. Kock and G. S. Markman, *Periodic, quasiperiodic, and chaotic motion in a forced predator–prey ecosystem*, in "Dynamical Systems and Environmental Models" (eds. H. G. Bothe, W. Ebeling, A. B. Kurzhanski and M. Peschel), Akademie-Verlag, Berlin, (1987), 95–104.
[30] T. Lindström, *Qualitative analysis of a predator–prey system with limit cycles*, J. Math. Biol., **31** (1993), 541–561.
[31] G. S. Medvedev, *Transition to bursting via deterministic chaos*, Phys. Rev. Lett., **97** (2006), 048102.
[32] T. Oksanen, L. Oksanen, M. Schneider and M. Aunapuu, *Regulation, cycles and stability in northern carnivore-herbivore systems: back to first principles*, Oikos, **94** (2001), 101–117.
[33] S. Pavlou and I. G. Kevrekidis, *Microbial predation in a periodically operated chemostat: a global study of the interaction between natural and externally imposed frequencies*, Math. Biosci., **108** (1992), 1–55.
[34] W. H. Press, S. A. Teukolsky, W. T. Vetterling and B. P. Flannery, "Numerical Recipes in C: the Art of Scientific Computing," Cambridge University Press, Cambridge, 1992.
[35] S. Rinaldi and S. Muratori, *Conditioned chaos in seasonally perturbed predator–prey models*, Ecol. Model., **69** (1993), 79–97.
[36] S. Rinaldi, S. Muratori and Y. Kutznetsov, *Multiple attractors, catastrophe and chaos in seasonally perturbed predator–prey communities*, Bull. Math. Biol., **55** (1993), 15–35.

[37] S. Rinaldi and M. Scheffer, *Geometric analysis of ecological models with slow and fast processes*, Ecosystems, **3** (2000), 507–521.
[38] J. Rinzel, *A formal classification of bursting mechanisms in excitable systems*, in "Mathematical Topics in Population Biology, Morphogenesis and Neurosciences" (eds. E. Teramoto and M. Yamaguti), Lecture Notes in Biomathematics **71**, Springer-Verlag, Berlin, (1987), 267–281.
[39] G. C. Sabin and D. Summers, *Chaos in a periodically forced predator–prey ecosystem model*, Math. Biosci., **113** (1992), 91–113.
[40] R. Seydel, "Practical Bifurcation and Stability Analysis: from Equilibrium to Chaos," Springer-Verlag, New York, 1994.
[41] M. E. Solomon, *The natural control of animal populations*, J. Anim. Ecol., **18** (1949), 1–35.
[42] D. Terman, *Chaotic spikes arising from a model of bursting in excitable membranes*, SIAM J. Appl. Math., **51** (1991), 1418–1450.
[43] P. Turchin and I. Hanski, *An empirically based model for latitudinal gradient in vole population dynamics*, Am. Nat., **149** (1997), 842–874.
[44] A. Vidal, *Stable periodic orbits associated with bursting oscillations in population dynamics*, in "Positive Systems, LNCIS" (eds. C. Commault and N. Marchand), Springer-Verlag, Berlin, (2006), 439–446.
[45] X. J. Wang and J. Rinzel, *Oscillatory and bursting properties of neurons*, in "Brain Theory and Neural Networks" (eds. M. A. Arbib), MIT press, Cambridge, (1995), 686–691.
[46] D. Xiao and K. F. Zhang, *Multiple bifurcations of a predator–prey system*, Discrete. Cont. Dyn-B., **8** (2007), 417–433.
[47] P. Yodzis, *Predator–prey theory and management of multispecies fisheries*, Ecol. Appl., **4** (1994), 51–58.

Received May 23, 2008; Accepted June 2, 2008.

E-mail address: justine@amath.washington.edu
E-mail address: kot@amath.washington.edu